Supplementary Information (SI) for Inorganic Chemistry Frontiers.


# Enhancing the performance of polyoxometalate-based memristors in harsh environments based on hydrogen bonding cooperative π-conjugation interaction

*Ming-Ze Meng, Yi-Qun Gao, Yi-Ping Chen*, Hao-Hong Li, Xiao-Hui Huang**

,

## Index

## 1. Experimental Procedures

### 1.1 Materials

All chemicals were used as purchased without further puriffcation. Water was deionised and distilled before use.

### 1.2 Measurements

Powder X-ray diffraction (PXRD) patterns were recorded on a Rigaku DMAX 2500 diffractometer with CuKα radiation (λ = 1.54056 Å). The simulated PXRD pattern was derived from the Mercury Version 4.3.0 software using the X-ray single crystal diffraction data. The infrared spectra were recorded using KBr pellets by a Scientiffc Nicolet IS50 in the 4000–500 $cm^{-1}$ range. Thermogravimetric analyses were performed on a Mettler Toledo TGA/SDTA 851e analyzer in an air-ffow atmosphere with a heating rate of 10 °C/ min at a temperature of 30–800 °C. For the determination of two dimensional correlation infrared spectroscopy (2D-COS-IR) under magnetic perturbation, a magnetic controller designed and produced by our group was used to control the magnetic regulation range of 5–50 MT, and the measurement interval of 5 MT to test the dynamics of the infrared spectra of compounds' functional groups under magnetic perturbation. Variable-temperature in situ infrared testing was performed on a PerkinElmer FT-IR Spectrometer Spectrum3 with a HARRICK ATC-024-3 as the temperature controller at a rate of 10°C/min. The instrument used for the determination of XPS (X-ray photoelectron spectroscopy) was an ESCALAB 250 photoelectron spectrometer from VG Corporation, USA, with Al-Kα as the target ray source. Electrical bistability measurement on FTO/VB/Ag device was executed on KEYSIGHT B2911A single channel digital source meter. The SEM images were taken on a Nano SEM 230 field-emission scanning electron microscope. Atomic force microscope (AFM) measurements were performed with a ScanAsyst mode on a Bruker Dimension ICON (probe: ScanAsyst-AIR).

### 1.3 Structure determinations

Diffraction intensity data for single crystals VB-1, VB-2, and VB-3 were collected on a Bruker APEX II CCD area diffractometer equipped with a ffne focus, 2.0 kW sealed tube X-ray source (Mo Kα radiation, λ = 0.71073 Á) operating at 293 K. The empirical absorption correction was based on equivalent reffections. Structures were solved by direct methods followed by successive difference Fourier methods. The computations were performed using SHELXL (full matrix least squares techniques) in the Olex2 package [1]. For all nonhydrogen atoms, anisotropical refinements were carried out while the hydrogen atoms were introduced in the geometrically calculated position. The residual electron density that could not be sensibly modeled as solvents or anions were removed via the application of the SQUEEZE function in PLATON. Crystallographic details have been listed in Table S1. Crystallographic data for the structural analysis have been deposited with the Cambridge Crystallographic Data Center CCDC reference numbers: 2375135, 2375136 and 2375137 for 1, 2, and 3 respectively.

### 1.4 Syntheses of compounds

**VB1**. $NH_4VO_3$ (0.2g), $H_3BO_3$ (0.8 g), $Ni(CH_3COO)_2$ (0.1 g) were added to ethanol (8 mL), then en (ethylenediamine) (0.3 mL), 1,3-diaminopropane (0.15 mL) and Formic acid (0.1mL) were added respectively, and stirred for 30min at room temperature. After that, the solution was transferred into a Teffon-lined reactor, heated at 160 ℃ for 7 days, and

gradually cooled to room temperature. Dark blue block crystals were obtained, washed with water, and dried at room temperature. Yield: 27.3 % (based on $NH_4VO_3$).

**VB2.** $NH_4VO_3$ (0.2g), $H_3BO_3$ (0.8 g), $Ni(CH_3COO)_2$ (0.1 g) were added to ethanol (8 mL), then en (ethylenediamine) (0.3 mL), 1,3-diaminopropane (1.5 mL) and Formic acid (0.1mL) were added respectively, and stirred for 30min at room temperature. After that, the solution was transferred into a Teffon-lined reactor, heated at 160 ℃ for 7 days, and gradually cooled to room temperature. Dark blue block crystals were obtained, washed with water, and dried at room temperature. Yield: 26.3 % (based on $NH_4VO_3$).

**VB 3.** $NH_4VO_3$ (0.2g), $H_3BO_3$ (0.8 g), $Li_2CO_3$ (0.1 g) were added to ethanol (5 mL), then en (ethylenediamine) (0.3 mL), 1,3-diaminopropane (1.5 mL) and Formic acid (0.1mL) were added respectively, and stirred for 30min at room temperature. After that, the solution was transferred into a Teffon-lined reactor, heated at 160 ℃ for 7 days, and gradually cooled to room temperature. Green block crystals were obtained, washed with water, and dried at room temperature. Yield: 25.1 % (based on $NH_4VO_3$).

### 1.5 Memory device fabrications and measurements

FTO-coated glass substrate was sequentially cleaned by ultrasonic in acetone, ethanol and deionized water for 20 min, and dried in an oven for 15 min at 110 ºC. The as-synthesized crystal (5 mg) was dispersed in 5 mL Water, and the suspension was coated on FTO substrates by spin coating method at 300 rpm for 10 s and 2000 rpm for 40 s, followed by annealing at 60 °C for 30 min. Finally, Ag pastes were deposited as the top electrodes through a shadow mask (500 μm width) with circular holes with a diameter about 0.1 cm.

## 2. Supplementary Tables

**Table S1.** Crystal data and structure refinement parameters for compounds **VB1, VB2, VB3.**

| Compound | 1 | 2 | 3 |
|---|---|---|---|
| Empirical formula | $C_{12}H_{66}B_{28}N_{12}Ni_2O_{74}V_{10}$ | $C_{27}H_{110}B_{26}N_{18}O_{70}V_{10}$ | $C_{13}H_{78}B_{26}Li_2N_{10}O_{70}V_{10}$ |
| Formula weight | 2492.26 | 2597.78 | 2299.19 |
| Temperature [K] | 293 | 293 | 293 |
| Crystal system | monoclinic | orthorhombic | orthorhombic |
| Space group | *C2/m* | *Pbcn* | *Pbcn* |
| *a* (Å) | 20.0146(19) | 27.2018(13) | 26.4843(12) |
| *b* (Å) | 25.470(2) | 16.3281(7) | 16.0720(7) |
| *c* (Å) | 12.7134(12) | 21.6011(9) | 20.8945(9) |
| *α*(deg) | 90 | 90 | 90 |
| *β*(deg) | 122.660(2) | 90 | 90 |
| γ(deg) | 90 | 90 | 90 |
| Volume [Å$^3$] | 5456.2(9) | 9594.2(7) | 8893.9(7) |
| Z | 2 | 4 | 4 |
| ρcalc [gcm$^{-3}$] | 1.517 | 1.798 | 1.717 |
| μ [mm$^{-1}$] | 1.252 | 1.050 | 1.117 |
| F(000) | 2480 | 5272 | 4608 |
| Crystal shape/colour | Block/Blue | Block/Green | Block/Green |
| Radiation | Mo$K_\alpha$ (λ=0.71073 Å) | Mo$K_\alpha$ (λ=0.71073 Å) | Mo$K_\alpha$ (λ=0.71073 Å) |
| 2θ range [°] | 4.83 to 50.18 (0.84 Å) | 4.23 to 50.02 (0.84 Å) | 3.55 to 50.05 (0.84 Å) |
| Index ranges | −22 ≤ h ≤ 23<br>−30 ≤ k ≤ 30<br>−15 ≤ l ≤ 15 | −21 ≤ h ≤ 22<br>−22 ≤ k ≤ 19<br>−23 ≤ l ≤ 17 | −31 ≤ h ≤ 31<br>−19 ≤ k ≤ 16<br>−24 ≤ l ≤ 24 |
| Reflections collected | 26044 | 16938 | 55544 |
| Independent reflections | 4915<br>$R_{int}$ = 0.0533<br>$R_{sigma}$ = 0.0426 | 1827<br>$R_{int}$ = 0.0223<br>$R_{sigma}$ = 0.0135 | 7855<br>$R_{int}$ = 0.0709<br>$R_{sigma}$ = 0.0520 |
| Completeness to θ = 25.089° | 98.7 % | 99.6 % | 99.9 % |
| Data / Restraints / Parameters | 4915/537/321 | 1827/12/108 | 7855/470/600 |
| Goodness-of-fit on F$^2$ | 1.087 | 0.996 | 1.099 |
| Final R indexes [I≥2σ(I)] | $R_1$ = 0.0938<br>w$R_2$ = 0.2198 | $R_1$ = 0.0866<br>$\omega R2$ = 0.3292 | $R_1$ = 0.0722<br>w$R_2$ = 0.2244 |
| Final R indexes [all data] | $R_1$ = 0.1016<br>w$R_2$ = 0.2245 | $R_1$ = 0.0897<br>$\omega R2$ = 0.3412 | $R_1$ = 0.1053<br>w$R_2$ = 0.2566 |
| Largest peak/hole[eÅ$^{-3}$] | 1.77/-1.67 | 2.68/-3.31 | 1.81/-0.77 |

[a] $R_1 = \sum||F_o|-|F_c||/\sum|F_o|$, [b] $\omega R_2 = \{\sum\omega[(F_o)^2-(F_c)^2]^2/\sum\omega[(F_o)_2]^2\}^{1/2}$.

**Table S2.** Selected bond lengths [Å] of **VB1.**

| Bond | Dist | Bond | Dist |
|---|---|---|---|
| Ni1–N1$^{\#1}$ | 2.132(9) | O4–B1 | 1.372(14) |
| Ni1–N1 | 2.132(9) | O5–B1 | 1.364(8) |
| Ni1–N2 | 2.107(8) | O5–B2 | 1.450(10) |
| Ni1–N2$^{\#1}$ | 2.107(8) | O6–B2 | 1.495(10) |
| Ni1–N3 | 2.110(8) | O7–B2 | 1.482(12) |
| Ni1–N3$^{\#1}$ | 2.110(8) | O7–B4 | 1.465(10) |
| N1–C1 | 1.483(14) | O8–B4 | 1.476(10) |
| N2–C2 | 1.443(14) | O9–B4 | 1.441(10) |
| N3–C3 | 1.459(14) | O9–B5 | 1.351(11) |
| C1–C2 | 1.535(16) | O10–B5 | 1.379(10) |
| C3–C3$^{\#1}$ | 1.49(2) | O11–B5 | 1.353(11) |
| V1–O1 | 1.585(6) | O11–B6 | 1.486(13) |
| V1–O4 | 1.986(5) | O12–B6 | 1.455(12) |
| V1–O6 | 1.914(5) | O12–B7 | 1.346(9) |
| V1–O13$^{\#3}$ | 1.919(5) | O13–B6 | 1.463(11) |
| V1–O14$^{\#4}$ | 1.985(5) | O14–B7 | 1.397(15) |
| V2–O2 | 1.595(6) | O15–B6 | 1.510(12) |
| V2–O6 | 1.935(5) | O15–B8 | 1.355(12) |
| V2–O8 | 1.962(5) | O16–B8 | 1.342(14) |
| V2–O10$^{\#3}$ | 1.992(5) | O17–B8 | 1.489(9) |
| V2–O13$^{\#3}$ | 1.960(5) | O18–B2 | 1.467(11) |
| V3–O3 | 1.612(9) | O18–B3 | 1.377(10) |
| V3–O8$^{\#3}$ | 1.933(5) | O19–B3 | 1.368(11) |
| V3–O8 | 1.933(5) | O19–B4 | 1.515(10) |
| V3–O10$^{\#3}$ | 1.963(5) | O20–B3 | 1.370(11) |
| V3–O10 | 1.963(5) | | |

Symmetry transformations used to generate equivalent atoms:
#1: 1-X, +Y, 2-Z; #2: +X, 1-Y, +Z; #3: 1-X, +Y, 1-Z; #4: 1-X, 1-Y, 1-Z

**Table S3.** Selected bond lengths [Å] of **VB2.**

| Bond | Dist | Bond | Dist | Bond | Dist |
|---|---|---|---|---|---|
| V1–O6 | 1.945(4) | O2–B2 | 1.482(8) | O28–B9 | 1.469(7) |
| V1–O6$^{\#1}$ | 1.945(4) | O3–B1 | 1.383(8) | O28–B11 | 1.448(8) |
| V1–O8 | 1.597(6) | O3–B13 | 1.492(8) | O29–B11 | 1.488(7) |
| V1–O9 | 1.954(4) | O4–B2 | 1.474(8) | O30–B10 | 1.370(9) |
| V1–O9$^{\#1}$ | 1.954(4) | O4–B13 | 1.456(8) | O31–B10 | 1.379(8) |
| V2–O5$^{\#1}$ | 1.939(4) | O5–B13 | 1.479(8) | O31–B11 | 1.495(8) |
| V2–O6$^{\#1}$ | 1.956(4) | O6–B2 | 1.492(8) | O32–B11 | 1.467(7) |
| V2–O9 | 1.994(4) | O7–B2 | 1.443(9) | O32–B12 | 1.347(7) |
| V2–O10 | 1.601(4) | O7–B3 | 1.347(8) | O33–B12 | 1.377(8) |
| V2–O12 | 1.935(4) | O9–B3 | 1.376(8) | O35–B12 | 1.364(8) |
| V3–O5$^{\#1}$ | 1.941(4) | O11–B3 | 1.368(8) | O35–B13 | 1.477(8) |
| V3–O12 | 1.942(4) | O11–B4 | 1.470(8) | N1–C1 | 1.488(7) |
| V3–O13 | 1.602(4) | O12–B4 | 1.479(8) | N1–B8 | 1.659(7) |
| V3–O16 | 1.944(4) | O14–B4 | 1.465(8) | N2–C3 | 1.500(8) |
| V3–O33$^{\#1}$ | 1.985(4) | O14–B5 | 1.334(8) | C1–C2 | 1.512(9) |
| V4–O16 | 1.923(4) | O15–B4 | 1.466(8) | C2–C3 | 1.503(8) |
| V4–O20 | 1.946(4) | O15–B6 | 1.454(8) | N3–C4 | 1.499(9) |
| V4–O29$^{\#1}$ | 1.946(4) | O16–B6 | 1.487(8) | C4–C5 | 1.519(9) |
| V4–O33$^{\#1}$ | 1.954(4) | O17–B5 | 1.375(8) | N6–C9 | 1.405(14) |
| V4–O34 | 1.595(4) | O17–B6 | 1.491(8) | N7–C11 | 1.571(13) |
| V5–O20 | 1.964(4) | O18–B5 | 1.386(8) | C9–C10 | 1.537(16) |
| V5–O22 | 1.953(4) | O19–B6 | 1.464(8) | C10–C11 | 1.484(15) |
| V5–O24$^{\#1}$ | 1.945(4) | O19–B7 | 1.360(7) | N4–C6 | 1.477(11) |
| V5–O26 | 1.601(4) | O20–B7 | 1.387(8) | N5–C8 | 1.409(13) |
| V5–O29$^{\#1}$ | 1.938(4) | O21–B7 | 1.349(8) | C6–C7 | 1.445(13) |
| V6–O22$^{\#1}$ | 1.927(4) | O21–B8 | 1.465(7) | C7–C8 | 1.572(14) |
| V6–O22 | 1.927(4) | O22–B8 | 1.451(7) | N8–C12 | 1.457(12) |
| V6–O24 | 1.948(4) | O23–B8 | 1.417(8) | N9–C14 | 1.458(11) |
| V6–O24$^{\#1}$ | 1.948(4) | O23–B9 | 1.446(8) | C12–C13 | 1.492(12) |
| V6–O25 | 1.613(5) | O24–B9 | 1.504(7) | C13–C14 | 1.534(12) |
| O1–B1 | 1.385(8) | O27–B9 | 1.495(8) | | |
| O2–B1 | 1.338(8) | O27–B10 | 1.351(8) | | |

Symmetry transformations used to generate equivalent atoms:
#1: 1-X, +Y, 1.5-Z

**Table S4.** Selected bond lengths [Å] of **VB3.**

| Bond | Dist | Bond | Dist | Bond | Dist |
|---|---|---|---|---|---|
| V1–O1 | 1.934(4) | O1–B14 | 1.430(8) | O22–B9 | 1.326(10) |
| V1–O1$^{\#1}$ | 1.934(4) | O3–B2 | 1.486(9) | O24–B9 | 1.382(9) |
| V1–O2 | 1.615(6) | O4–B2 | 1.435(9) | O25–B9 | 1.383(10) |
| V1–O3$^{\#1}$ | 1.946(4) | O4–B14 | 1.434(8) | O25–B10 | 1.462(9) |
| V1–O3 | 1.946(4) | O4–Li1 | 1.989(13) | O26–B10 | 1.477(9) |
| V2–O1$^{\#1}$ | 1.945(4) | O5–B2 | 1.528(8) | O27–B10 | 1.479(9) |
| V2–O3 | 1.952(4) | O5–B3 | 1.351(9) | O27–B11 | 1.337(9) |
| V2–O9 | 1.604(5) | O5–Li1 | 2.072(13) | O28–B11 | 1.392(9) |
| V2–O36 | 1.939(4) | O6–B3 | 1.376(9) | O29–B11 | 1.359(8) |
| V2–O33$^{\#1}$ | 1.994(4) | O7–B3 | 1.366(8) | O29–B12 | 1.523(8) |
| V3–O36 | 1.926(4) | O7–B4 | 1.501(8) | O29–Li1$^{\#2}$ | 1.990(13) |
| V3–O11 | 1.618(5) | O35–B10 | 1.455(9) | O30–B12 | 1.489(9) |
| V3–O13 | 1.961(4) | O35–B12 | 1.422(9) | O32–B12 | 1.450(8) |
| V3–O30$^{\#1}$ | 1.938(4) | O8–B2 | 1.449(8) | O32–B13 | 1.357(8) |
| V3–O33$^{\#1}$ | 1.952(4) | O8–B4 | 1.440(9) | O33–B13 | 1.371(8) |
| V4–O15 | 1.924(4) | O36–B4 | 1.497(9) | O34–B13 | 1.349(8) |
| V4–O20 | 1.605(5) | O12–B4 | 1.468(8) | O34–B14 | 1.482(8) |
| V4–O21 | 1.953(5) | O12–B5 | 1.350(8) | N3–C7 | 1.485(8) |
| V4–O24$^{\#1}$ | 1.977(4) | O13–B5 | 1.388(9) | N3–B14 | 1.630(9) |
| V4–O26$^{\#1}$ | 1.924(4) | O14–B5 | 1.363(8) | C4–C7 | 1.540(11) |
| V5–O21 | 1.932(4) | O14–B6 | 1.497(8) | C4–C3 | 1.494(10) |
| V5–O21$^{\#1}$ | 1.932(4) | O15–B6 | 1.477(8) | N5–C3 | 1.579(12) |
| V5–O23 | 1.618(7) | O16–B6 | 1.494(8) | Li1–O10 | 1.989(15) |
| V5–H23$^{\#1}$ | 2.043(7) | O16–B7 | 1.375(9) | N1–C1 | 1.499(9) |
| V5–O24 | 1.953(4) | O17–B7 | 1.347(9) | C2–C1$^{\#1}$ | 1.506(9) |
| V5–O24$^{\#1}$ | 1.953(4) | O18–B7 | 1.352(9) | C2–C1 | 1.506(9) |
| V6–O13$^{\#1}$ | 1.982(4) | O18–B8 | 1.508(9) | N6–C6 | 1.386(13) |
| V6–O15$^{\#1}$ | 1.929(4) | O19–B6 | 1.433(9) | N7–C5 | 1.577(18) |
| V6–O26 | 1.922(4) | O19–B8 | 1.433(9) | C6–C5 | 1.462(15) |
| V6–O30 | 1.953(4) | O21–B8 | 1.506(9) | | |
| V6–O31 | 1.619(5) | O22–B8 | 1.466(10) | | |

Symmetry transformations used to generate equivalent atoms:
#1: 1-X, +Y, 0.5-Z; #2: 1-X, 1-Y, 1-Z

**Table S5.** Hydrogen bonding parameters of **VB1**.

| D-H···A | d(D-H) | d(H···A) | d(D···A) | <(DHA) | Symmetry codes of A |
|---|---|---|---|---|---|
| N1-H1A···O20($B^b$-$O_t$) | 0.86 | 2.15 | 2.943 | 155 | -0.5-x,1.5-y,-z |
| O16-H2A···O9($B^a$-$O_\mu$) | 0.88 | 2.34 | 2.781 | 132 | 1-x,y,2-z |
| O20-H3C···O19($B^b$-$O_\mu$) | 0.89 | 1.76 | 2.668 | 174 | 0.5-x,1.5-y,1-z |
| O17-H3B···O11($B^a$-$O_\mu$) | 0.89 | 2.21 | 2.903 | 135 | 1-x,0.5+y,0.5-z |
| N3-H1B···O18($B^b$-$O_\mu$) | 0.86 | 2.29 | 2.979 | 149 | 0.5+x,1.5-y,1+z |
| C2-H2D···O2(V-$O_t$) | 0.97 | 2.23 | 3.076 | 154 | 0.5-x,1.5-y,1-z |

**Table S6.** Hydrogen bonding parameters of **VB2**.

| D-H···A | d(D-H) | d(H···A) | d(D···A) | <(DHA) | Symmetry codes of A |
|---|---|---|---|---|---|
| O18-H18A···O2($B^a$-$O_\mu$) | 0.93 | 1.91 | 2.801(5) | 159.0 | 1-x,-y,1-z |
| O18-H18B···N4 | 0.93 | 2.20 | 2.899(7) | 131.2 | 1-x,1-y,1-z |
| O30-H30B···O3($B^a$-$O_\mu$) | 0.93 | 1.76 | 2.678(5) | 168.4 | 1.5-x,0.5+y,+z |
| N2-H2A···O11($B^a$-$O_\mu$) | 0.89 | 2.00 | 2.834(7) | 156.1 | 1-x,-y,1-z |
| N2-H2···O1W | 0.89 | 2.01 | 2.844(8) | 156.0 | -0.5+x,1.5-y,1-z |
| O1W-H1WA···N2 | 0.85 | 2.23 | 2.844(8) | 129.4 | 0.5+x,1.5-y,1-z |
| N3-H3E···O4($B^a$-$O_\mu$) | 0.89 | 1.91 | 2.792(6) | 169.9 | x, y, z |
| N3-H3D···O15($B^a$-$O_\mu$) | 0.89 | 1.88 | 2.737(6) | 160.8 | x, y, z |
| N6-H6E···O35($B^a$-$O_\mu$) | 0.89 | 2.06 | 2.803(8) | 139.7 | x, y, z |
| N6-H6C···O1W | 0.89 | 1.95 | 2.771(11) | 152.0 | 1.5-x,-0.5+y,+z |
| N7-H7E···O17($B^a$-$O_\mu$) | 0.89 | 1.83 | 2.718(7) | 175.5 | 0.5+x,0.5-y,1-z |
| N4-H4A···O18($B^b$-$O_t$) | 0.89 | 2.10 | 2.899(7) | 149.2 | 1-x,1-y,1-z |
| N4-H4B···O25(V-$O_t$) | 0.89 | 2.08 | 2.845(6) | 143.9 | x, y, z |
| N5-H5C···N9 | 0.89 | 2.07 | 2.885(10) | 150.9 | 1.5-x,1.5-y,0.5+z |
| N8-H8E···O1W | 0.89 | 1.87 | 2.725(11) | 159.2 | x, y, z |
| N9-H9A···O31(V-$O_t$) | 0.89 | 2.03 | 2.888(7) | 162.2 | +x,1-y,-0.5+z |
| N9-H9C···N5 | 0.89 | 2.04 | 2.885(10) | 157.0 | 1.5-x,1.5-y,-0.5+z |
| O1-H1B···O31($B^a$-$O_\mu$) | 0.93 | 2.03 | 2.939 | 166 | 1.5-x,-0.5+y,+z |
| N7-H7D···O27($B^a$-$O_\mu$) | 0.89 | 2.07 | 2.944 | 170 | 1.5-x,-0.5+y,+z |
| N4-H4C···O27($B^a$-$O_\mu$) | 0.89- | 2.07 | 2.971 | 172.5 | x,y,z |

**Table S7.** Hydrogen bonding parameters of **VB3**.

| D-H···A | d(D-H) | d(H···A) | d(D···A) | <(DHA) | Symmetry codes of A |
|---|---|---|---|---|---|
| O6-H1a···O16($B^a$-$O_\mu$) | 0.82 | 1.86 | 2.656 | 166 | 0.5-x,0.5+y,z |
| O2-H1b···O23(V-$O_t$) | 0.86 | 2.29 | 2.711 | 149 | x,1+y,z |
| N1-H2a···O19($B^a$-$O_\mu$) | 0.89 | 1.91 | 2.794 | 170 | x, y, z |
| O28-H3c···O18($B^a$-$O_\mu$) | 0.93 | 1.90 | 2.811 | 167 | x, y, z |
| N1-H1b···O35($B^a$-$O_\mu$) | 0.89 | 1.88 | 2.749 | 165 | x, y, z |
| N6-H3b···O2(V-$O_t$) | 0.86 | 2.15 | 2.993 | 136 | x, y, z |
| N5-H5b···O22($B^a$-$O_\mu$) | 0.89 | 2.06 | 2.849 | 147 | 1-x,1-y,1-z |
| N6-H6a···O28($B^b$-$O_t$) | 0.86 | 2.18 | 2.863 | 137 | x, y, z |
| O17-H17···O7($B^a$-$O_\mu$) | 0.82 | 2.00 | 2.800 | 163 | -0.5+x,-0.5+y,0.5-z |
| N5-H2a···O25($B^a$-$O_\mu$) | 0.89 | 2.16 | 2.960 | 149 | x,1+y,z |
| N6-H23···O23(V-$O_t$) | 0.86 | 2.37 | 3.051 | 138 | x, y, z |

**Note**：$B^a$-O ($BO_4$), $B^b$-O ($BO_3$), V-$O_t$: vanadium terminated oxygen bond; V-$O_\mu$: vanadium bridge oxygen bond, Ow: free water.

**Table S8.** Valence calculation of vanadium atom in **VB1**.

| Atoms | V1 | V2 | V3 | Average |
|---|---|---|---|---|
| BVS | 4.255 | 4.141 | 4.178 | 4.193 |

**Table S9.** Valence calculation of vanadium atom in **VB2**.

| Atoms | V1 | V2 | V3 | V4 | V5 | V6 | Average |
|---|---|---|---|---|---|---|---|
| BVS | 4.193 | 4.179 | 4.214 | 4.264 | 4.215 | 4.228 | 4.215 |

**Table S10.** Valence calculation of vanadium atom in **VB3.**

| Atoms | V1 | V2 | V3 | V4 | V5 | V6 | Average |
|---|---|---|---|---|---|---|---|
| BVS | 4.207 | 4.119 | 4.162 | 4.230 | 4.146 | 4.197 | 4.176 |

**Table S11.** A performance comparison of FTO/VB3/Ag with some known POMs-based memory devices.

| Devices structure | Set /Reset (V) | Endurance | ON/OFF ratio | Temperature tolerant | ON/OFF ratio(max temperature) | Memory effect | Ref. |
|---|---|---|---|---|---|---|---|
| ITO/$Na_{10}(H_2O)_{36}[Co_2(phen)_2(4,4'-bipy)(Nb_6O_{19})_2]\cdot 19H_2O$/Ag | 1.12/−7 | 200 | $1.18 \times 10^3$ | 70℃ | $1.15 \times 10^2$ | Binary RRAM | **[2]** |
| ITO/ $Na_6V_{10}O_{28}$/Cr/Au | 1.2/0.8 | 200 | 25 | - | - | Unipolar RRAM | **[3]** |
| ITO/$\{[Co_2(bpdo)_4(H_2O)_6](\alpha\text{-}GeW_{12}O_{40})\}\cdot 4(H_2O)\}_n$/Ag | 1.77/−3.42 | 100 | $1.18 \times 10^2$ | 150℃ | $3.5 \times 10^3$ | Binary RRAM | **[4]** |
| ITO/$H_4[Na(H_2O)_5]2[Co^{II}(en)_3]_2\{[Co^{III}(en)]_2(Ta_6O_{19})_2\}\cdot 22H2O$ /Ag | 3.79/−7.64 | 100 | $1.43 \times 10^3$ | - | - | Binary RRAM | **[5]** |
| ITO/$[Co(H_2O)_6]_2[Co_3(bpdo)_4(H_2O)_{10}][Co_4(H_2O)_2(B\text{-}aPW_9O_{34})_2]\cdot 2bpdo\cdot 14H_2O$ /Ag | -0.63/0.75 | 20 | 27.3 | 270℃ | 55 | Binary RRAM | **[6]** |
| ITO/$(MV)_2[Cu_2I_3](MnMo_6O_{18}L_2)\cdot 4CH_3CN$ /Ag | 0.97/-3.49 | 700 | $2.32 \times 10^2$ | 240℃ | $6.2 \times 10^2$ | Binary RRAM | **[7]** |
| ITO/$H_3PW_{12}O_{40}$@PMMA/Au | 1.2/-1.71 | 100 | $6\times 10^2$ | - | - | Binary RRAM | **[8]** |
| ITO/$\{Ni^{II}(1,4\text{-cby})_2[H_2(\gamma\text{-}Mo_8O_{26})]\}\cdot 4H_2O$/Ag | 1.2/-0.90 | 30 | 700 | 100℃ | $7\times 10^2$ | Binary RRAM | **[9]** |
| FTO/VB1/Ag | 0.82 | 120 | $6.67\times 10^3$ | - | - | Binary WORM | **This work** |
| FTO/VB2/Ag | 0.79 | 100 | $1.07\times 10^4$ | - | - | Binary WORM | **This work** |
| FTO/VB3/Ag | 1.07/-6.94 | 130 | $2.62\times 10^4$ | 270℃ | $1.55 \times 10^3$ | Binary RRAM | **This work** |

## Supplementary Figures and Scheme

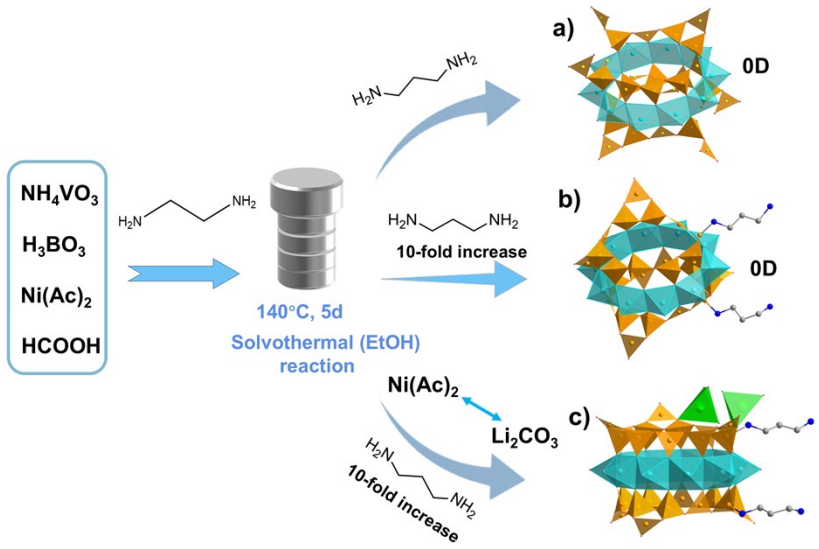


**Scheme. S1.** Synthetic process of **1-3**, a) VB1, b) VB2, c) VB3.

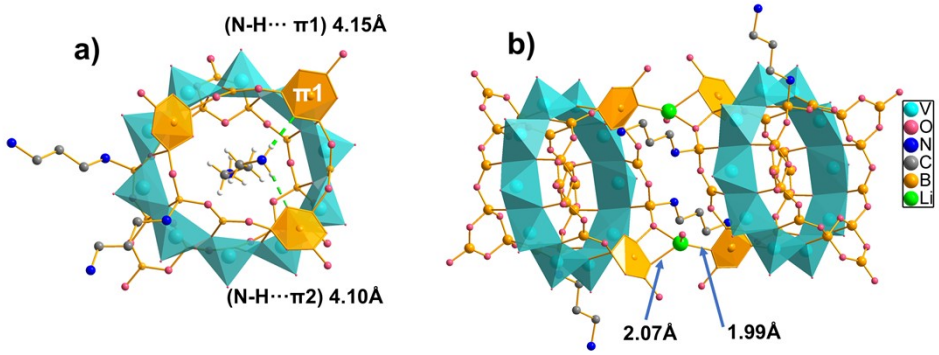


**Figure S1.** a) $\pi$-conjugated structures in $[V_{10}B_{26}O_{28}(1,3dap)_2]^{n-}$, b) Linking $[B_3O_6]$ conjugated units by Li-O bonds.

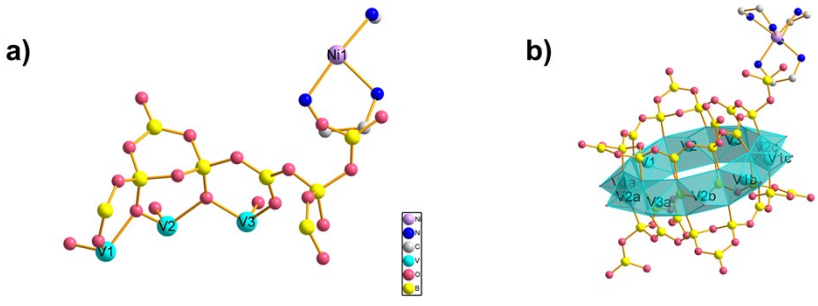


**Figure S2.** a) The asymmetric unit of **VB1**. b) The coordination environment of **VB1**, symmetric of code: a: x, 1-y, z; b: 1-x,1-y,1-z; c: 1-x,-y,1-z.

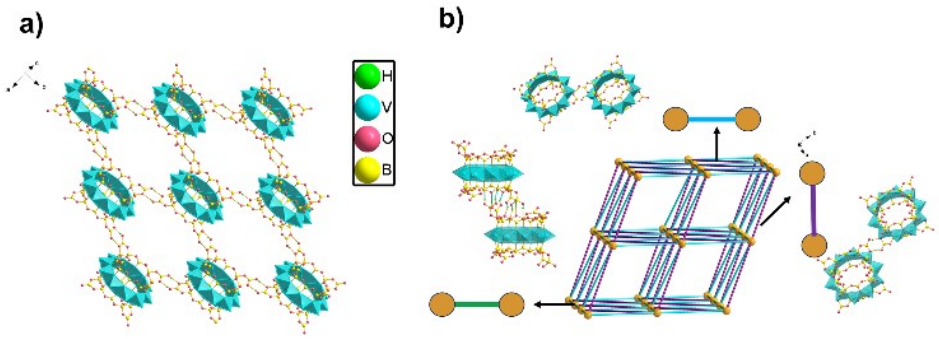


**Figure S3.** a) Two-dimensional layered structure of **VB1**. b) Three-dimensional supramolecular structure of VB1, topological symbol of $\{3^{12}.4^{28}.5^{5}\}$.

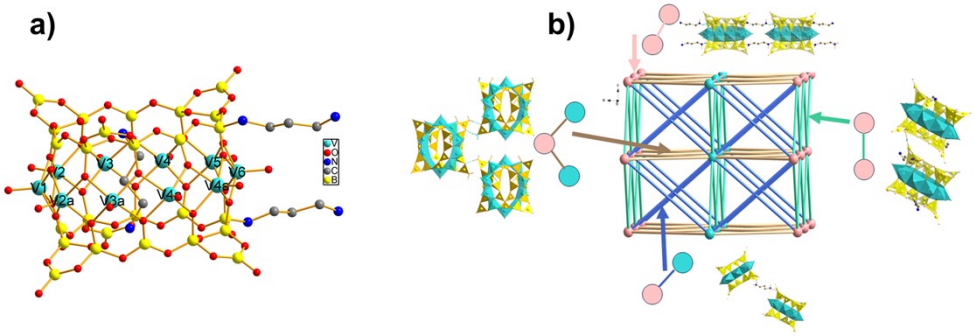


**Figure S4.** a) The coordination environment of **VB2**, symmetric of code: a: 1-x, y, 3/2-z. b) Three-dimensional supramolecular structure of **VB2**, topological symbol of $\{3^{36}.4^{48}.5^{7}\}$.

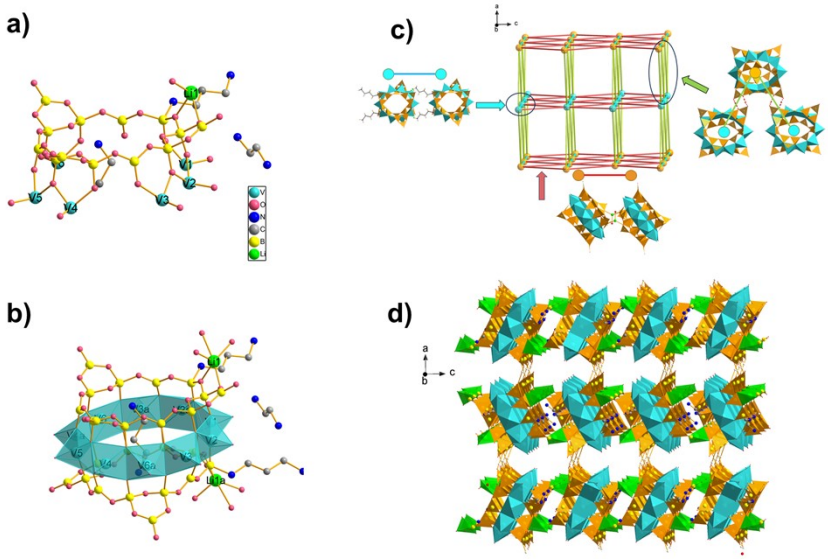


**Figure S5.** a) The asymmetric unit of **VB3**. b) The coordination environment of **VB3**, symmetric of code: a: 1-x, y, 1/2-z. c) Three-dimensional supramolecular structure of **VB3**, topological symbol of $\{3^{12}.4^{28}.5^{5}\}$. d) View of the 3D porous framework of **VB3.**

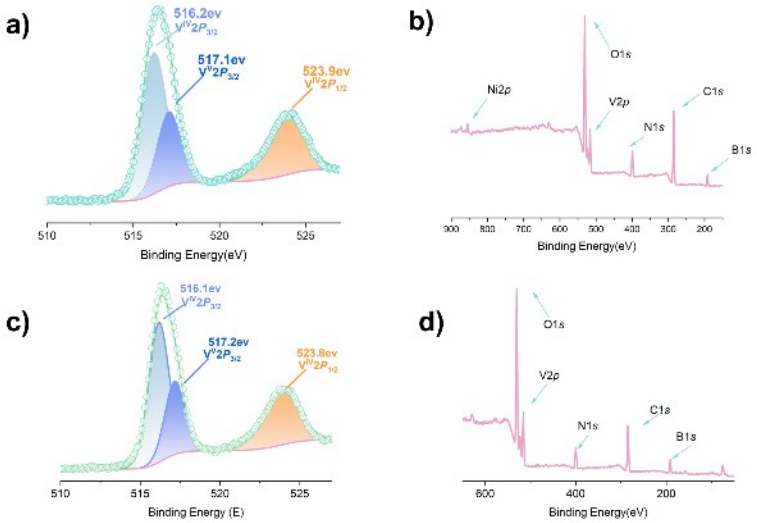


**Figure S6.** a, b) The XPS spectrum of **VB1**. c, d)The XPS spectrum of **VB2**.

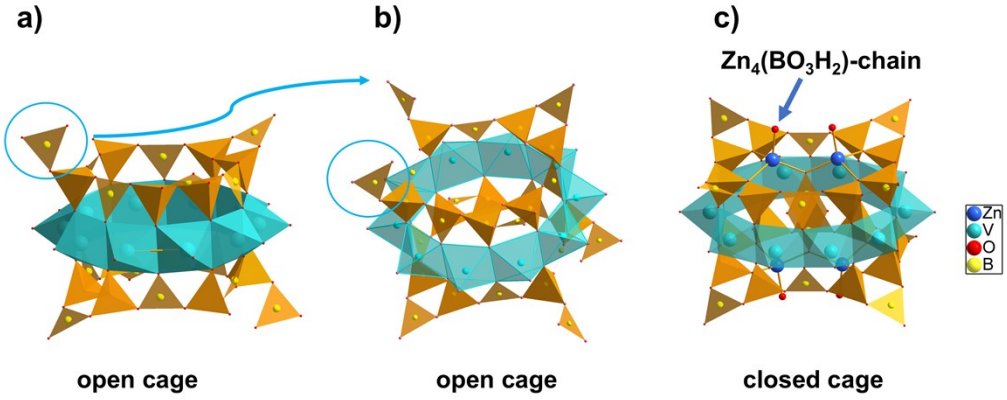


**Figure S7. a**) $[V_{10}B_{26}O_{70}]^{22-}$. b) $[\beta\text{-}V^{IV}_{8}V^{V}_{2}B_{28}O_{74}]^{22-}$ in VB1. (c) $[Zn_4(BO_3)V_{10}B_{28}O_{74}]^{11-}$.

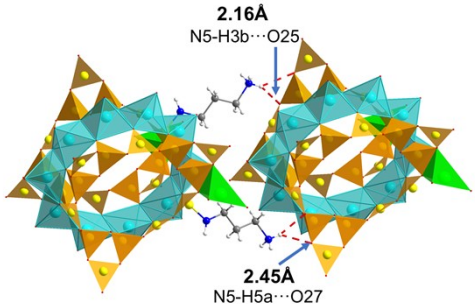


**Figure S8.** Hydrogen bonding at the 1, 3 dap ligand on cluster cages of **VB2** and **VB3.**

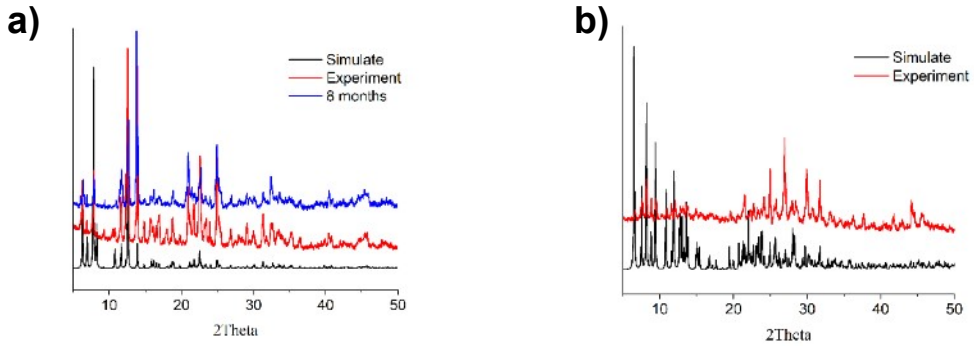


**Figure S19.** Powder X-ray diffraction (PXRD) patterns of a) VB1 and b) VB2.

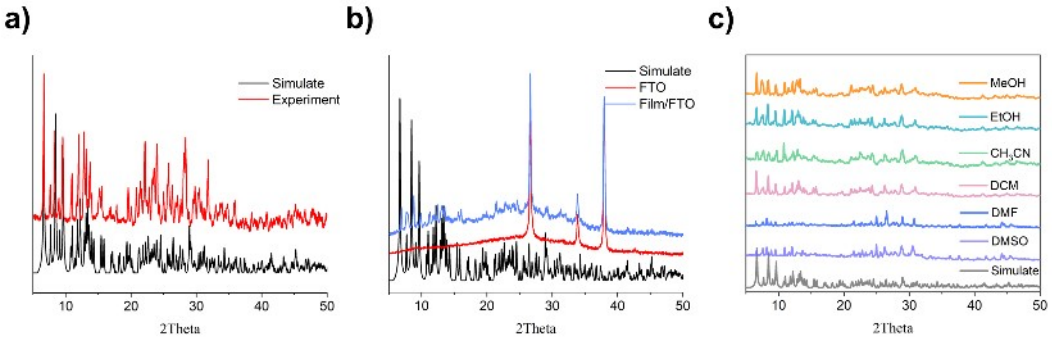


**Figure S10.** a) PXRD patterns of VB3. b) on FTO. c) PXRD patterns after soaking in solvents.

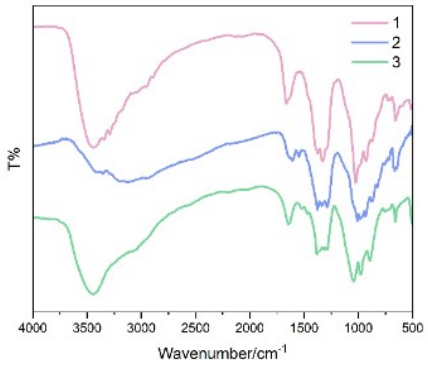


**Figure S11.** IR spectra of **VB1, VB2** and **VB3.** In the IR spectra of **VB1**, **VB2**, and **VB3**, there are strong peaks at 972 $cm^{-1}$, and 862 $cm^{-1}$ attributable to the $\nu_{as}(V{=}O_t)$, $\nu_s(V{=}O_t)$ for **VB1** and 930 $cm^{-1}$, 866 $cm^{-1}$ for **VB2**, and 973 $cm^{-1}$, 887 $cm^{-1}$ for **VB3**. Due to the $\nu_{as}(V\text{-}O_\mu)$ or $\nu_s(V\text{-}O_\mu)$, there are strong peaks at 754 $cm^{-1}$, 721 $cm^{-1}$ for **VB1**, at 730 $cm^{-1}$ for **VB2**, and at 761 $cm^{-1}$ for **VB3**. The vibrational peaks of the cluster cage skeleton of the three compounds were in the range of 600 $cm^{-1}$-650 $cm^{-1}$. In addition, there are strong peaks at

1025cm$^{-1}$, 1328cm$^{-1}$ ascribed to the $\nu_{as}$($B^a$-O) and $\nu_{as}$($B^b$-O) for **VB1**, and 1009 cm$^{-1}$, 1378 cm$^{-1}$ for **VB2,** and 1044 cm$^{-1}$, 1383 cm$^{-1}$ for **VB3**. ($B^a$-O: B-O bond of $BO_4$; $B^b$-O: B-O bond of $BO_3$; V=$O_t$: vanadium end oxygen bond; V-$O_\mu$: vanadium bridge oxygen bond). The bands at 1650 cm$^{-1}$-1500 cm$^{-1}$ and 3000−3500 cm$^{-1}$ can be ascribed to the bending and stretching vibrations of $\nu$(O-H) and $\nu$(N-H).

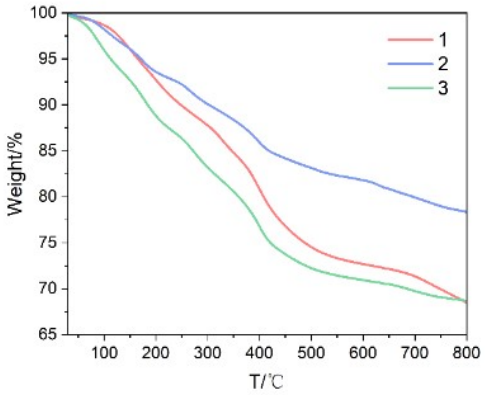


**Figure S12.** TG curves of **VB1**, **VB2** and **VB3**. The TG curves indicate that the weight loss of VB1 from room temperature to about 420°C is due to the loss of free $[Ni(en)_3]^{2+}$ complexs in the structure (calculated:19.68%, observed: 20.27%), followed by the collapse of the overall skeleton. The weight loss of VB2 from room temperature to about 80°C is due to the loss of lattice water molecules (calculated:1.41%, observed: 1.27%), followed by successive weight loss up to 480°C due to the loss of free 1,3-diaminopropane molecules (calculated:17.11%, observed: 15.87%), after which the overall skeleton collapses after 500°C. The weight loss of VB3 from room temperature to 70°C is due to the loss of the coordinated water molecules (calculated:1.56%, observed: 1.67%), and the weight loss from 100°C to 220°C is due to the loss of free ethylenediamine molecules and free 1,3-diaminopropane molecules (calculated: 8.69%, observed: 8.40%), and the subsequent successive weight loss is due to the loss of coordinated ions until the whole skeleton collapses at around 400°C.

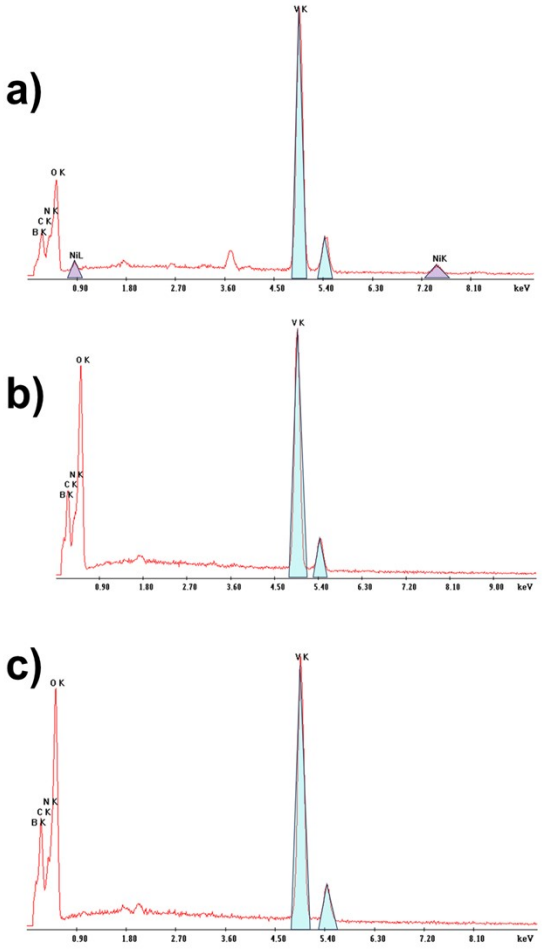


**Figure S13.** Energy dispersive X-ray (EDS) spectrum of (a)VB1 and (b) VB2 (c) VB3.

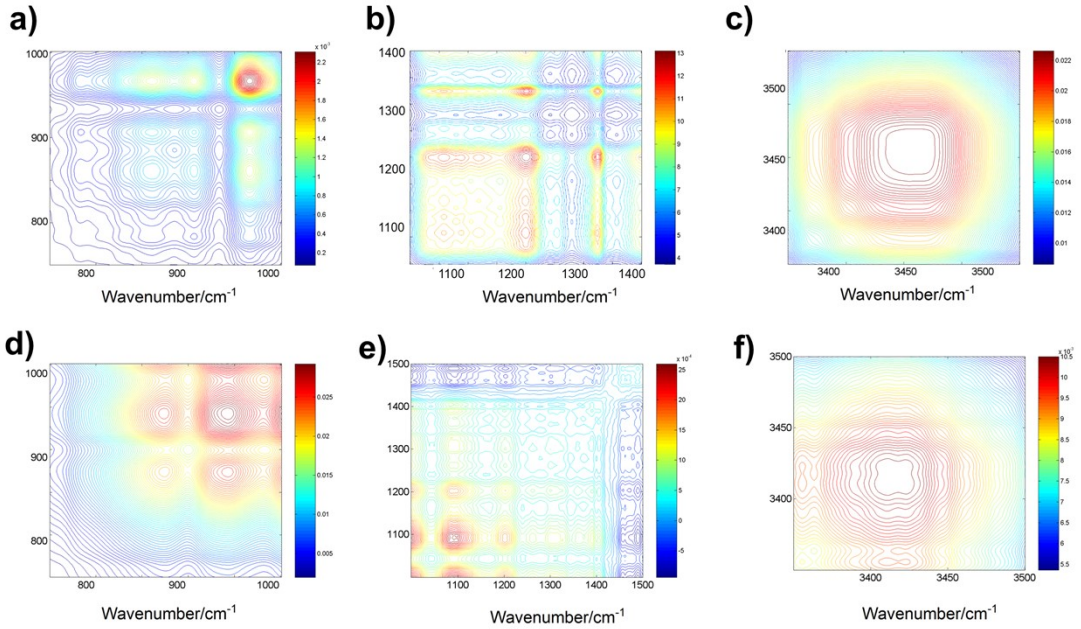


**Figure S14.** a-c) Two-dimensional correlation infrared spectra of **VB1**. d-f) Two-dimensional correlation infrared spectra of **VB2**. The strong response peaks appeared at $\nu_{as}(V{=}O_t)$ (980 $cm^{-1}$) for VB1, which is related to the hydrogen bonding (C2-H2D···O2) formed at the vanadium terminal oxygen in the structure of VB1. The strong response peaks appeared at $\nu_{as}(V{=}O_t)$ (950 $cm^{-1}$) for VB2, which is related to the hydrogen bonding (N4-H4B···O25, N9-H9A···O31) formed at the vanadium terminal oxygen in the structure of VB2. Meanwhile, VB2,VB3 have similar cluster structures, and VB3 has a strong response peak at $\nu_{as}(B^b\text{-}O_t)$ (1380 $cm^{-1}$) (Figure 2b), but it is found that the response peak of VB2 is weak at this position., probably due to the weak $\pi$- conjugation at $[B_3O_6]$ units in VB2.

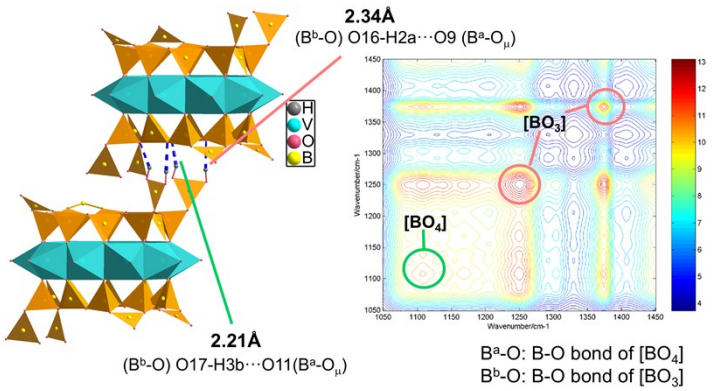


**Figure S15.** Hydrogen bonding at the modified $[BO_3]$ group on **VB1** and its response on the 2D-COS spectrum.

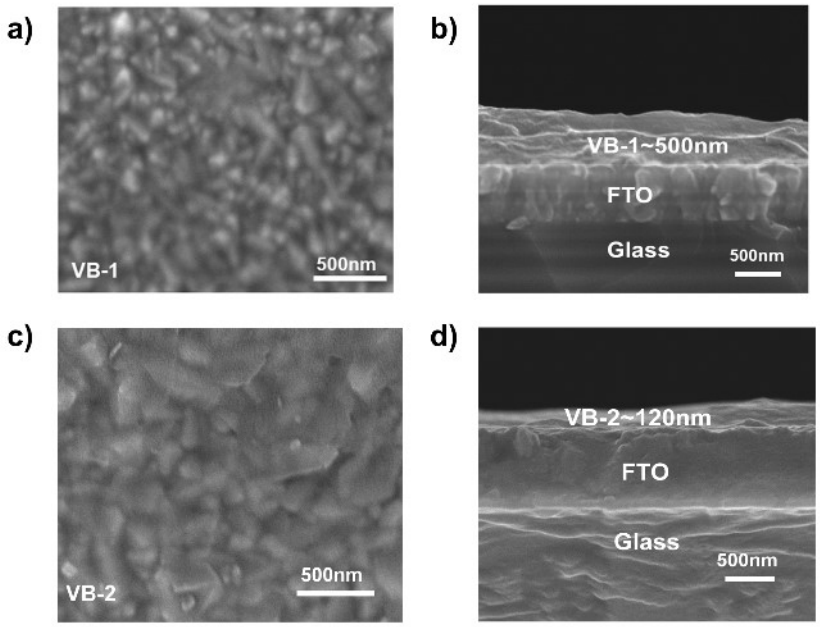


**Figure S16.** a) The surface SEM images and b) cross-sectional of the FTO/VB1/Ag memory device (the **VB1** film: ~500 nm), (c) and (d) The FTO/VB2/Ag (the **VB2** film: ~120 nm)

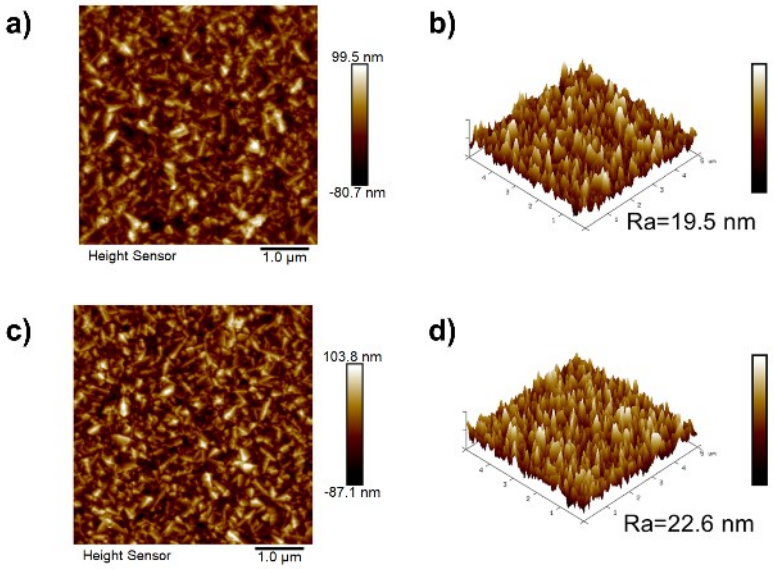


**Figure S17.** a) 2D and b) 3D topography AFM images of **VB1** film. c) 2D and d) 3D topography AFM images of **VB2** film.

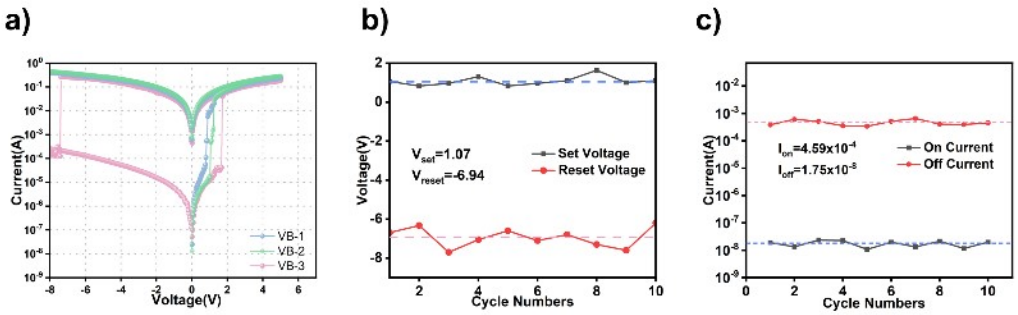


**Figure S18.** a) *I–V* characteristics of Devices **1**, **2** and **3**. b) $V_{SET}$/$V_{RESET}$ variation of 10 random sample FTO/VB-3/Ag devices at HRS and LRS states. c) Stabilities of 10 random samples of FTO/VB-3/Ag device at HRS and LRS states (read at 0.01V).

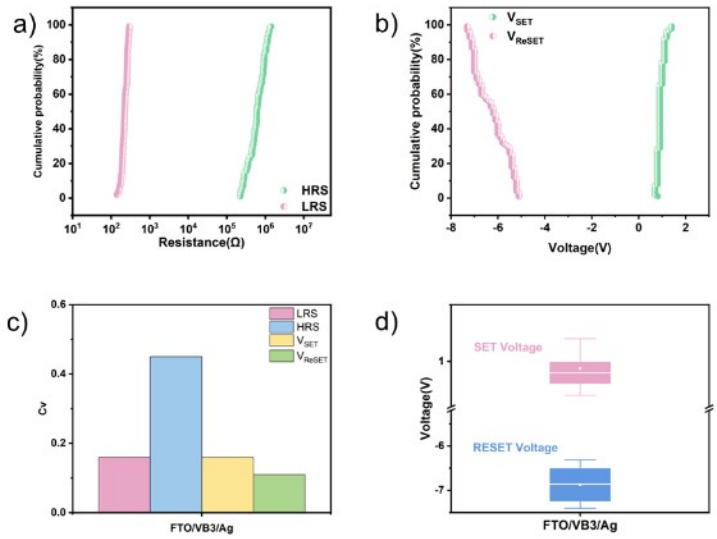


**Figure S19.** a) The cumulative probability (CP) distributions of the HRS and LRS values for the FTO/VB-3/Ag device b) The cumulative probability (CP) distributions plot of the $V_{SET}$ and $V_{RESET}$ values. c) Cv of FTO/VB-3/Ag devices. d) SET/RESET voltage distributions of the FTO/VB-3/Ag device.

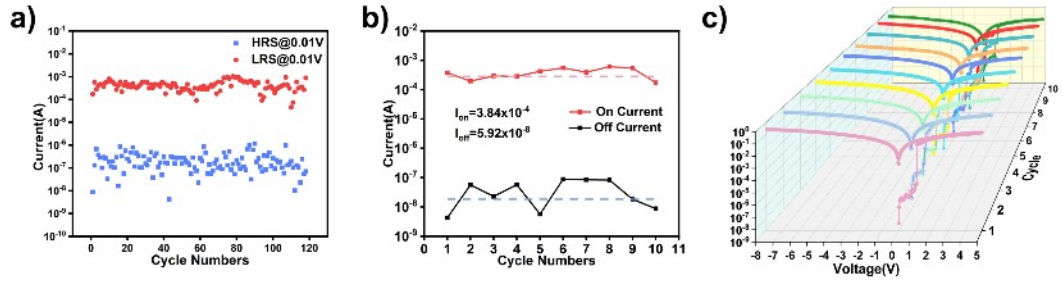


**Figure S20.** Performance of VB1 based film memristors: a) Switching durability with 120 consecutive cycles. b) Stabilities of 10 random samples of FTO/VB1/Ag device at HRS and LRS states (read at 0.01V). c) The current-voltage (*I-V*) curves of 10 random samples.

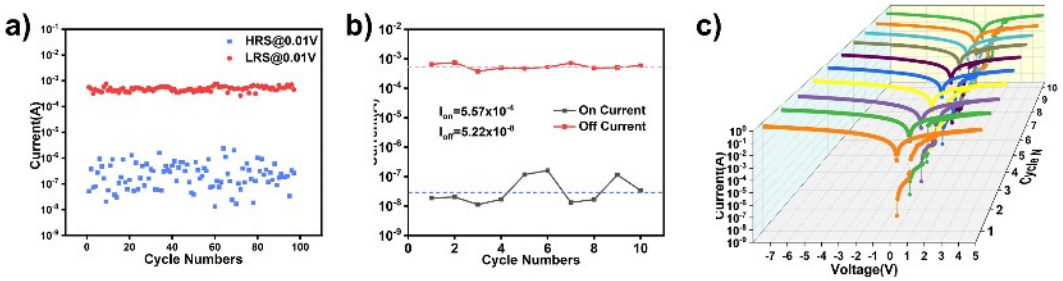


**Figure S21.** Performance of VB2 based film memristors: a) Switching durability with 100 consecutive cycles. b) Stabilities of 10 random samples of FTO/VB2/Ag device at HRS and LRS states (read at 0.01V). c) The current-voltage (*I-V*) curves of 10 random samples.

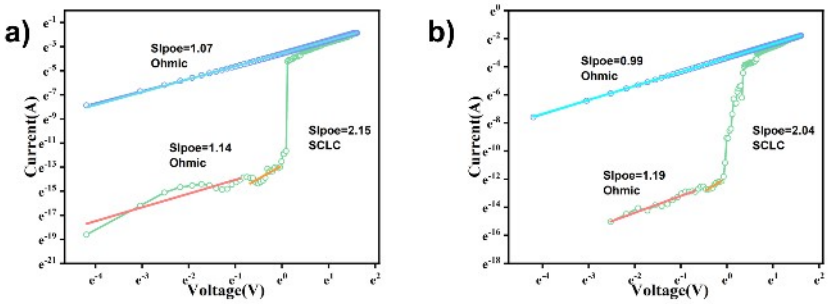


**Figure S22** a) The log I-log V fitting curves of FTO/VB1/Ag memristor in positive sweeping. b) The log I-log V fitting curves of FTO/VB2/Ag memristor in positive sweeping.

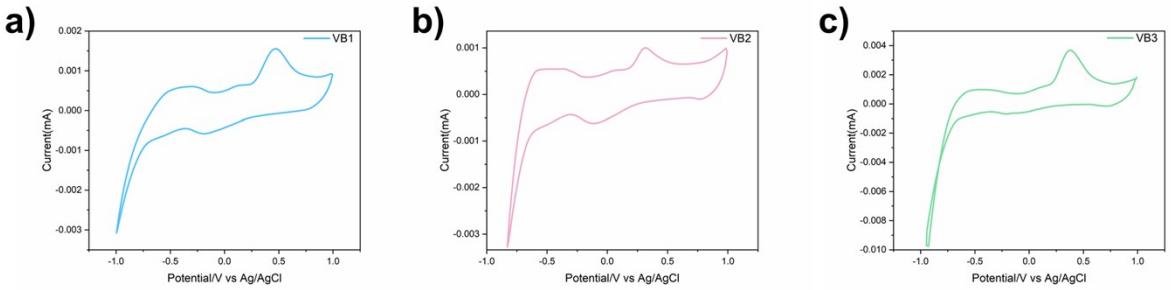


**Figure S23.** CV curves of (a)VB1; (b)VB2; (c)VB3.

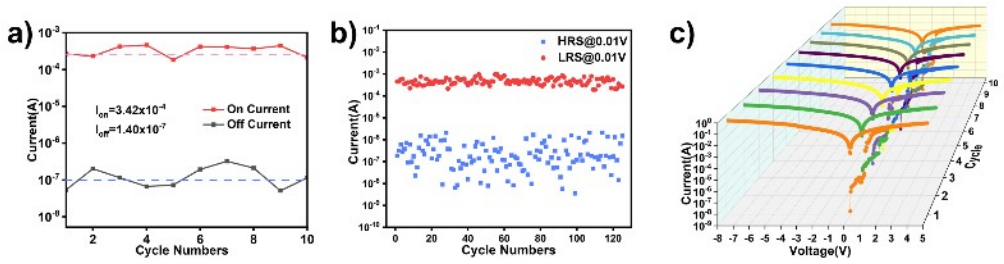


**Figure S24.** Performance of VB3 based film memristors (0.5 mg/mL): a) Stabilities of 10 random samples of FTO/VB3/Ag device at HRS and LRS states (read at 0.01V). b) Switching durability with 125 consecutive cycles. c) The current-voltage (*I*-*V*) curves of 10 random samples.

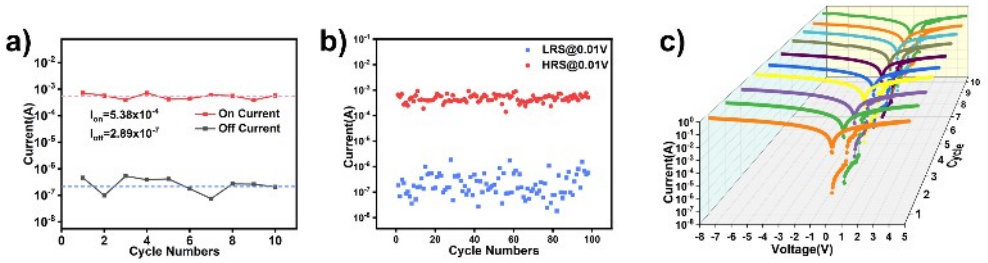


**Figure S25.** Performance of VB3 based film memristors (2 mg/mL): a) Stabilities of 10 random samples of FTO/VB3/Ag device at HRS and LRS states (read at 0.01V). b) Switching durability with 100 consecutive cycles. c) The current-voltage (*I*-*V*) curves of 10 random samples.

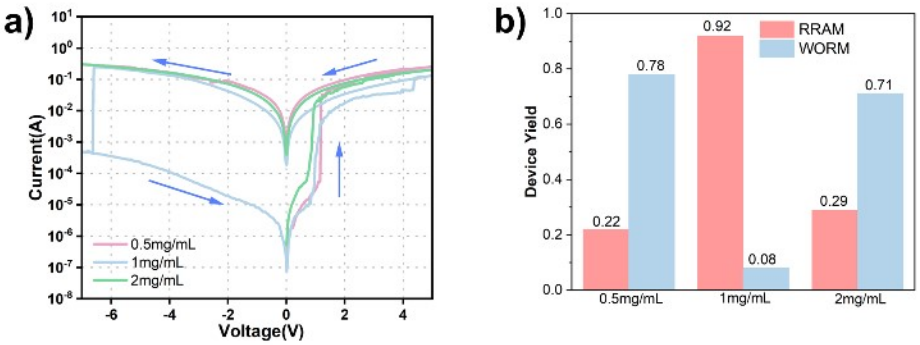


**Figure S26.** a) Comparison of typical current-voltage (*I*-*V*) curves for films made with VB3 at different concentrations. b) The device yields of FTO/VB3/Ag device fabricated at different concentrations.

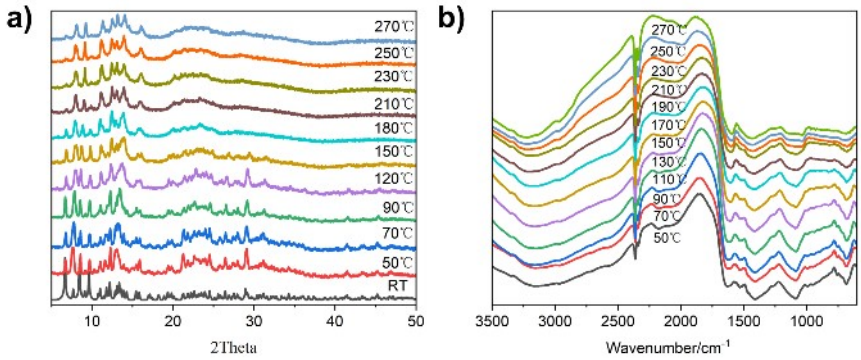


**Figure S27.** a) and b) Temperature-dependent PXRD and IR spectra of **VB3**.

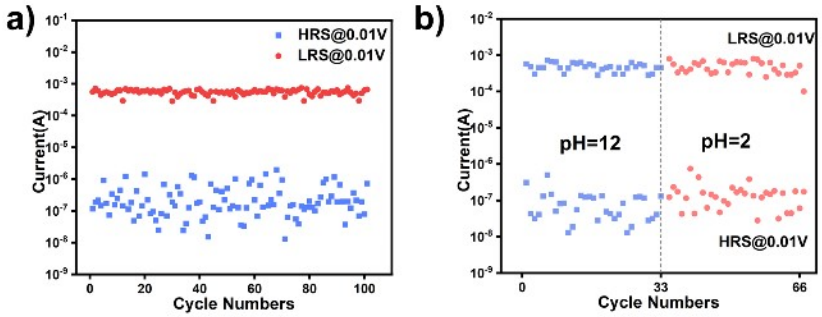


**Figure S28.** a) Device stability of FTO/VB3/Ag after 8 months (100 consecutive cycles). b) Device endurance after soaked in acidic and alkaline aqueous solution for 2 h.

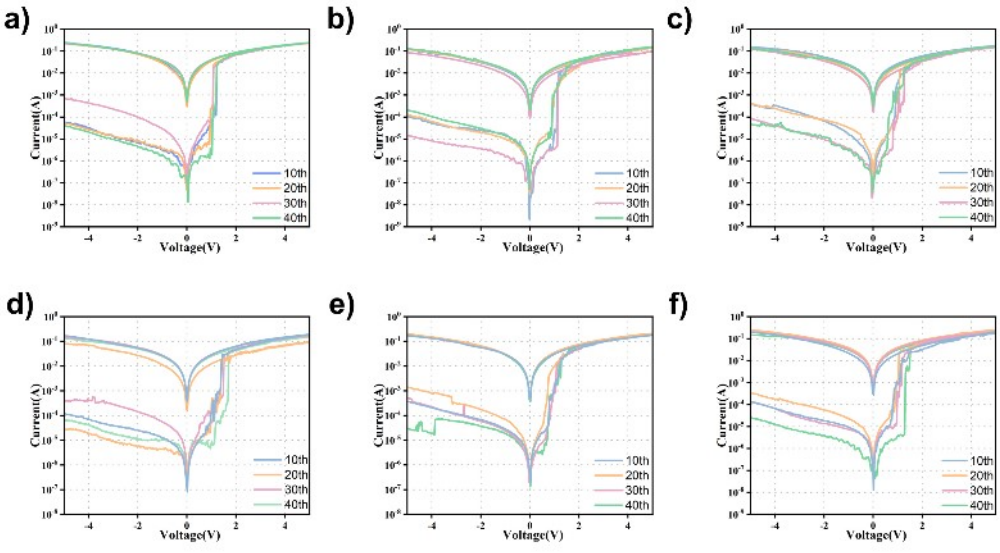


**Figure S29.** Device endurance after soaked in various organic solvents for 2 h: (a) $CH_3CN$. (b) EtOH. (c) MeOH. (d) DMSO. (e) DMF. (f) DCM.

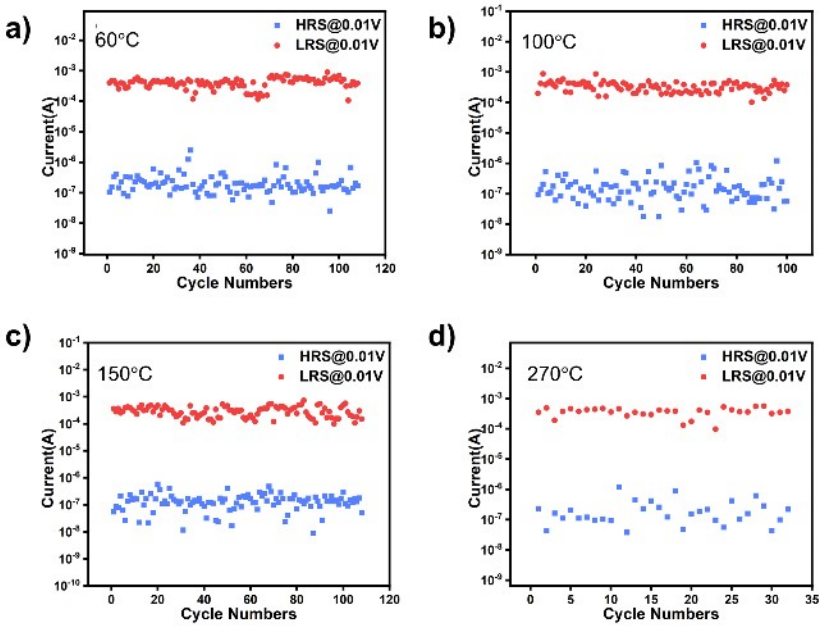


**Figure S30.** Temperature tolerant performance of FTO/VB3/Ag memory device at different temperature: (a) 110 cycles at 60 °C; (b) 100 cycles at 100 °C; (d) 110 cycles at 150 °C; (e) 32 cycles at 270 °C.

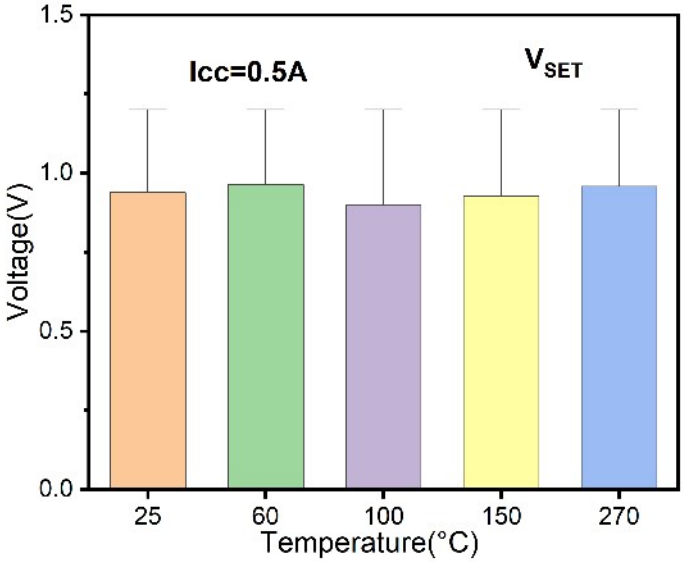


**Figure S31** The corresponding distributions of $V_{SET}$ at different temperatures of 25, 60, 100, 150 and 270 °C.

**References**

[1] O. V. Dolomanov, L. J. Bourhis, R. J. Gildea, J. A. K. Howard, H. Puschmann, *J. Appl. Crystallogr.* **2009**, *42*, 339−341.

[2] Y.-J. Wang, N. Shi, C. Sun, Y.-Q. Sun, S.-T. Zheng, *Inorg. Chem.* **2023**, *62*, 10675−10683.

[3] S. N. S, N. Basu, M. Cahay, S. M. N, S. S. Mal, P. P. Das, *Phys. Status Solidi A.* **2020**, *217, 2000306*.

[4] B. Chen, Y.-R. Huang, K.-Y. Song, X.-L. Lin, H.-H. Li, Z.-R. Chen, *Chem. Mat.* **2021**, *33*, 2178-2186.

[5] Y.-F. Cao, Y. Lin, X.-X. Li, Y.-Q. Sun, S.-T. Zheng, *Crystengcomm.* **2024**, *26*, 3527-3534.

[6] Y. R. Huang, X. L. Lin, B. Chen, H. D. Zheng, Z. R. Chen, H. H. Li, S. T. Zheng, *Angew. Chem. Int. Ed.* **2021**, *60*, 16911-16916.

[7] H.-B. Chen, M.-Y. He, T. Li, C.-C. Deng, H.-P. Xiao, M.-Q. Qi, X.-J. Kong, H.-H. Li, X.-X. Li, S.-T. Zheng, *J. Mater. Chem. C.* **2024**, *12*, 13555-13561.

[8] X. Chen, P. Huang, X. Zhu, S. Zhuang, H. Zhu, J. Fu, A. S. Nissimagoudar, W. Li, X. Zhang, L. Zhou, Y. Wang, Z. Lv, Y. Zhou, S.-T. Han, *Nanoscale Horiz.* **2019**, *4*, 697-704.

[9] S. Yu, A. Tian, Q. Lu, X. Xu, S. Ma, X. Wang, Z. Wang, *Inorg. Chem.* **2023**, *62*, 1549-1560.